MRS Advances (2021) 6:535–539
https://doi.org/10.1557/s43580-021-00118-w

ORIGINAL PAPER

Room temperature PVD TiN to improve the ferroelectric properties of HZO films in the BEoL

David Lehninger[1] · Konstantin Mertens[1] · Lukas Gerlich[1] · Maximilian Lederer[1] · Tarek Ali[1] · Konrad Seidel[1]

Received: 12 April 2021 / Accepted: 26 July 2021 / Published online: 6 August 2021
© The Author(s) 2021

Abstract
Zirconium-doped hafnium oxide (HZO) crystallizes at low temperatures and is thus ideal to implement ferroelectric (FE) functionalities into the back end of line (BEoL). Therefore, metal-ferroelectric-metal (MFM) capacitors are of great interest. Placed in the BEoL, they can be connected either to the drain- or the gate-contact of a standard logic device to realize different emerging FE-embedded non-volatile memory (eNVM) concepts. However, the low crystallization temperature increases also the risk for a premature crystallization of the HZO films during the growth of the top electrode (TE), in particular, if high-temperature processes like atomic layer deposition (ALD) or chemical vapor deposition (CVD) are used. Herein, the TE is deposited at room temperature via physical vapor deposition (PVD). The impact of different process gas flows on the FE properties of the HZO films is studied by X-ray diffraction and polarization versus electric field measurements.

Introduction

New applications like smart and energy-saving sensors for intelligence at the edge require the use of novel embedded non-volatile memory (eNVM) concepts, which combine the properties of high speed and low power together with good reliability characteristics [1]. Ferroelectric (FE) eNVMs are a promising approach to meet these requirements [2]. The non-volatility is enabled by the two remanent polarization states (P_r+, P_r−) instigated by the displacement of ions in a non-centrosymmetric crystal lattice. In the region of the coercive field ($|E_c|$), the polarization of the FE materials is switchable between both states [3].

Metal-ferroelectric-metal (MFM) capacitors are of great interest for FE eNVM concepts. Integrated into the back end of line (BEoL), they can be connected either to the drain- or the gate-contact of a standard logic to realize FE random access memories (FeRAMs) or a FE field effect transistors (FeFETs), respectively [2].

A crucial part for the successful BEoL integration is the thermal budget of the utilized materials and processes. The most promising FE material to meet these requirements is zirconium-doped hafnium oxide (HZO) [4–6]. It crystallizes in the FE phase at about 350 °C and over a wide range of doping concentrations [7–10].

Although the low crystallization temperature is a key enabler for the BEoL integration, it increases simultaneously the risk for the HZO crystallization during the growth of the top electrode (TE), in particular, if high-temperature processes like chemical vapor deposition (CVD) are used. It is known that such an in-situ crystallization (i.e., without fully developed TE) degrades the FE properties of the HZO [11].

Physical vapor deposition (PVD), like reactive magnetron sputtering, is beneficial to deposit the TE [12]. It is fast, low-cost, reproducible, and can be done at room temperature, which prevents an in-situ crystallization of the HZO.

Herein, the impact of the TE deposited via radio frequency (rf) reactive magnetron sputtering using various process gas (N_2, Ar) flows on the FE properties of HZO films embedded in TiN/FE/TiN MFM capacitors is presented.

Experimental

The MFM capacitors were deposited on highly boron-doped 300 mm silicon wafers with industry standard production tools.

The TiN bottom electrode of 10 nm thickness was deposited at 450 °C via atomic layer deposition (ALD) employing the precursors $TiCl_4$ and NH_3. The 10 nm HZO film was also deposited via ALD at 300 °C using $HfCl_4$ and $ZrCl_4$

✉ David Lehninger
David.Lehninger@ipms.fraunhofer.de

[1] Fraunhofer IPMS - Center Nanoelectronic Technologies (CNT), An der Bartlake 5, 01109 Dresden, Germany

as precursors together with H_2O as the oxidizing reactant and Ar as purging gas. The hafnium-to-zirconium ratio of 1:1 was achieved by using a precursor cycling ratio of 1:1.

The TiN TE was fabricated by rf reactive magnetron sputtering within an Applied Materials® Endura® Clover™ chamber using a metallic Ti target and pure N_2 or mixed Ar/N_2 plasma. Different film composition were realized by using various gas flows. The process time was constant. To keep the deposition temperature close to room temperature, the chuck was not heated. For comparison, a MFM structure with a CVD TiN TE (10 nm thickness, deposited at 400 °C using $TiCl_4$ and NH_3 as precursor and N_2 as purge gas) was fabricated and characterized as well.

To characterize the PVD TiN films, reference wafers were coated with TiN using the same processes as for the TE in the MFM capacitors. The bow and the film thickness were measured on these reference wafers by spectroscopic ellipsometry. The change in the wafer bow was calculated by subtracting the bow measured pre by the one measured post TiN deposition.

To crystallize the HZO films, all MFM capacitors (with the PVD and with the CVD TE) were post deposition annealed at 400 °C in N_2 atmosphere using rapid thermal annealing (RTA) with a hold time of 60 s, a ramp up rate of 50 Ks^{-1}, and passive cool down.

The structural characteristics of the HZO films embedded in the MFM capacitors were concluded from X-ray powder diffraction experiments in a glancing-angle diffraction geometry.

For the electrical measurements, Ti/Pt dots were patterned by using shadow mask and electron beam evaporation. To form individual MFM capacitors with areas from 0.007 to 0.15 mm^2, the TiN between the dot-contacts was removed by wet chemical etching using SC-1 clean.

Polarization versus electric field (P–E) measurements were performed with an aixACCT TF 3000 FE analyzer using a triangular waveform at a frequency of 1 kHz.

Results and discussion

Figure 1 displays the thickness of the TiN films (box plots) and the change in wafer bow (box charts) for various process gas flows. The film thickness decreases (i.e., the deposition rate decreases) with increasing N_2 flow. This can be attributed to a poisoning of the target and/or to the increased plasma density reducing the mean free path of the specimens.

The change in wafer bow is an indicator for the stress induced by the deposited film. It clearly increases if the TiN thickness grows. However, a significant influence on the composition of the process gas was not found. This indicates that all deposited TiN films are sutured with nitrogen. Also,

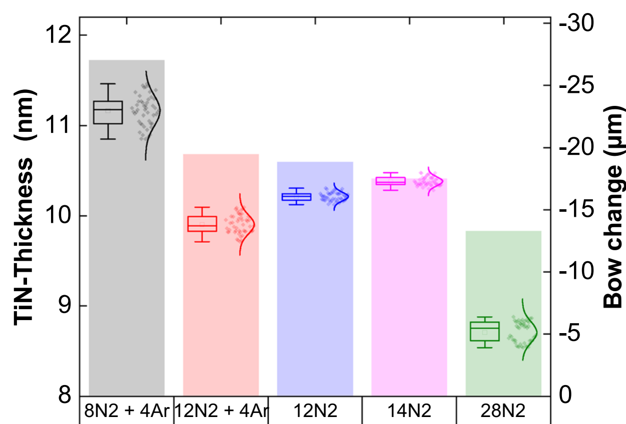

Fig. 1 Thickness (box plots) and changes in wafer bow (bar plots) for PVD TiN films deposited at different process gas flows on reference wafers. The respective process gas flow is given at the bottom of the figure in standard cubic centimeter per minute (sccm)

X-ray photoelectron spectroscopy (XPS) measurements indicate no significant deviation of the nitrogen content for all deposited films (data not shown).

Figure 2 depicts glancing-angle X-ray diffraction (GAXRD) pattern of the HZO films embedded in MFM capacitors with PVD TiN TE deposited at different process gas conditions. The thermal budget of 400 °C and 60 s is sufficient to crystallize all HZO films. The XRD pattern do not show diffraction lines that can be attributed to the non-FE monoclinic phase and no significant differences can be observed between the process gas flows. Only the sample with the TiN TE deposited at 12 sccm N_2 and 4 sccm Ar stands a bit out, since the integrated intensity of the [001] and [010] reflections (located at about 35° 2θ; see black arrow in Fig. 2) is increased. Due to the higher crystallographic texture of these FE and ferroelastic axes, a large remanent polarization (P_r) is expected for this capacitor [13, 14].

However, solely from XRD, it is not straightforward to distinguish between the cubic, the tetragonal, and the desired FE orthorhombic phase, because all the mentioned phases have reflection lines at similar 2θ angles. Therefore, and to attain an understanding of the FE film properties, electrical measurements were conducted (Fig. 3).

All capacitors with CVD or PVD TE show promising FE characteristics with similar shape of the polarization versus electric field (P–E) curves. In the pristine state, an anti-ferroelectric-like behavior can be observed. However, the pinching of the P–E characteristics disappears after field cycling due to the wake-up effect [13].

An important parameter of the HZO films is the robustness against leakage. The amount of leakage can be estimated qualitatively from the shape of the P–E characteristics, since high leakage leads to a "cigar-like" widening

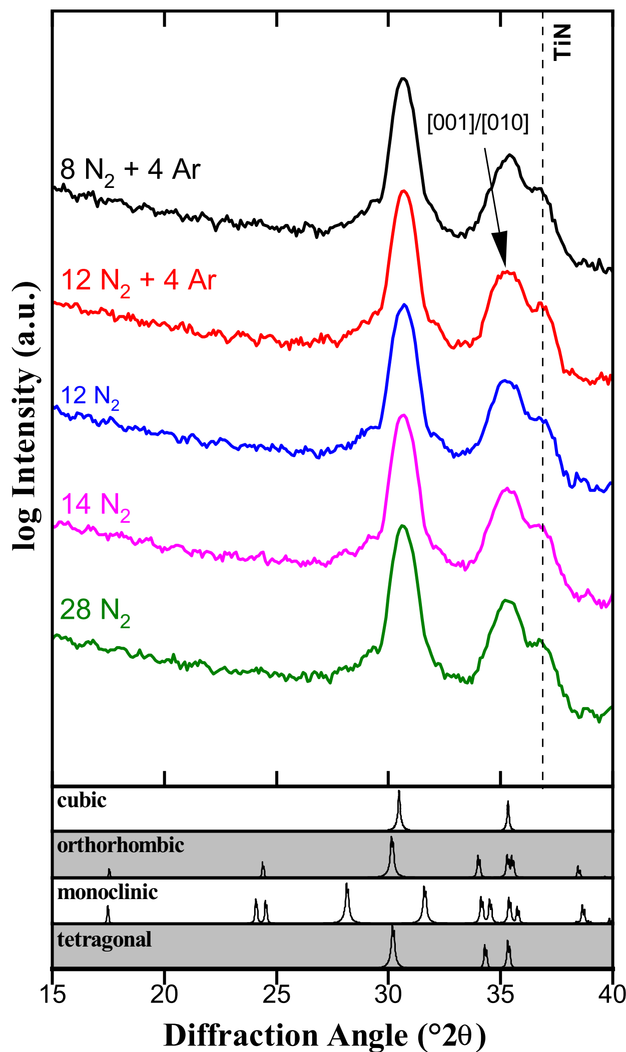

Fig. 2 GAXRD pattern of MFM capacitors with PVD TE deposited at different process gas flows given in sccm at the respective XRD pattern. All samples were annealed at 400 °C for 60 s in an RTP-type oven. At the bottom of the figure, the positions of the diffraction lines of individual HfO_2 phases are shown. In addition, the positions of the TiN diffraction line are added by a dashed vertical line

of the hysteresis loop [15]. None of the test structures show increased leakage, which is another indicator that all deposited TiN TE are saturated with nitrogen. If a sub-stoichiometric (i.e., rather metallic) TiN film is in direct contact with the HZO, interface reactions (like the scavenging of oxygen atoms) are expected to occur, which significantly increases the leakage.

Figure 4 shows the remanent polarization (P_r+) extracted from the P–E characteristics in Fig. 3. Devices with PVD TiN TE have significantly higher P_r+ than devices with CVD TiN TE. This is most likely due to the premature crystallization of the HZO film during the CVD TiN TE deposition at elevated temperatures (400 °C). Since the HZO crystallizes in the letter case without fully developed TE, which is important to stabilize the FE (orthorhombic) phase, the fraction of the none-FE (monoclinic) phase is significantly increased. Unfortunately, we do not have XRD data to proof this.

In the case of the PVD TiN TE, P_r+ increases significantly (within the examined range) if the N_2 flow is enlarged and/or if additional Ar is added to the process gas. However, a clear link between the measured P_r+ and the stress induced by the TE (cf. change in the wafer bow; Fig. 1) cannot be observed. The highest P_r+ was measured for the device with PVD TiN TE, which showed also the higher crystallographic texture of the FE and ferroelastic axis in Fig. 2.

Conclusion

The impact of the TiN TE and its deposition process on the FE properties of HZO films embedded in MFM structures was presented. All test devices with CVD or PVD TiN TE (last-mentioned deposited at different process gas flows) showed FE characteristics after post deposition annealing at 400 °C. However, devices with PVD TiN TE had significantly larger P_r+ as devices with CVD TiN TE. This difference was attributed to an in-situ crystallization of the HZO film during the CVD TE deposition at elevated temperatures. With respect to P_r and leakage current resistance of the test devices, the PVD TiN process presented here is promising for the integration of FE functionalities into the BEoL. It is fast, low-cost, reproducible, and can be done at room temperature.

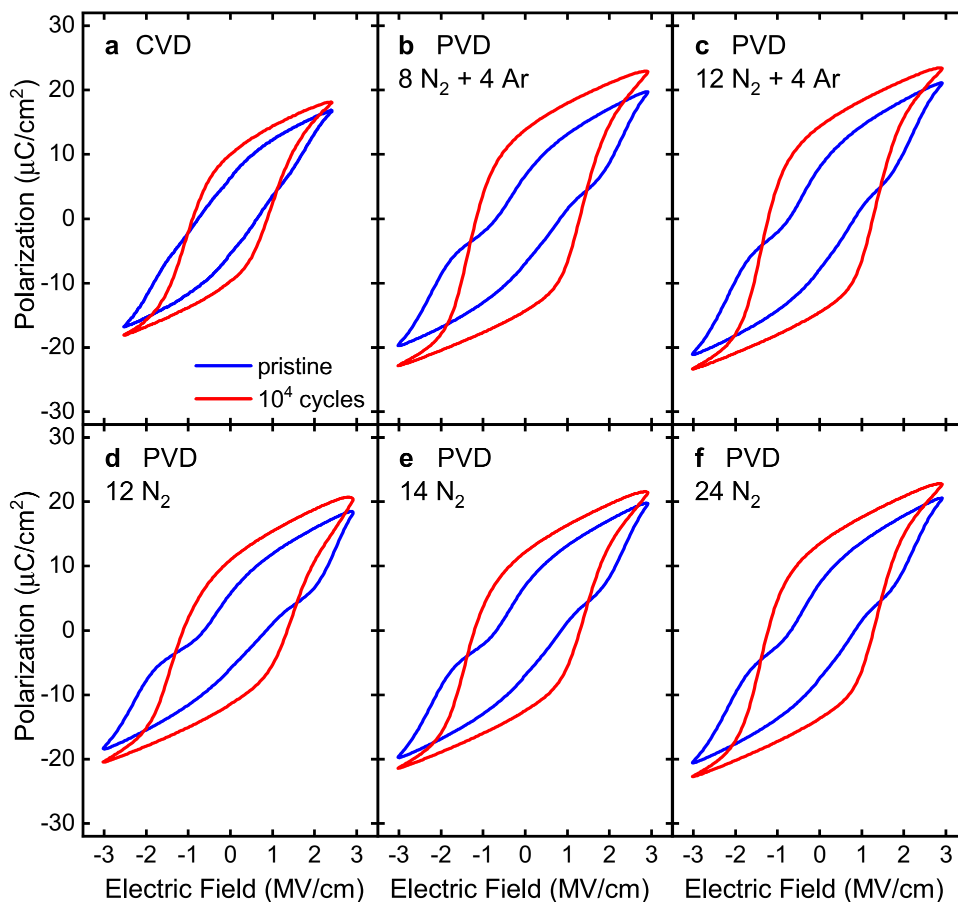

Fig. 3 P–E characteristics of MFM capacitors with different TiN TE in pristine state and after 10^4 field cycles for wake-up. The TiN TE was deposited either via **a** CVD or **b**–**f** PVD. In the latter case, the different gas flows are given in sccm within the respective graph

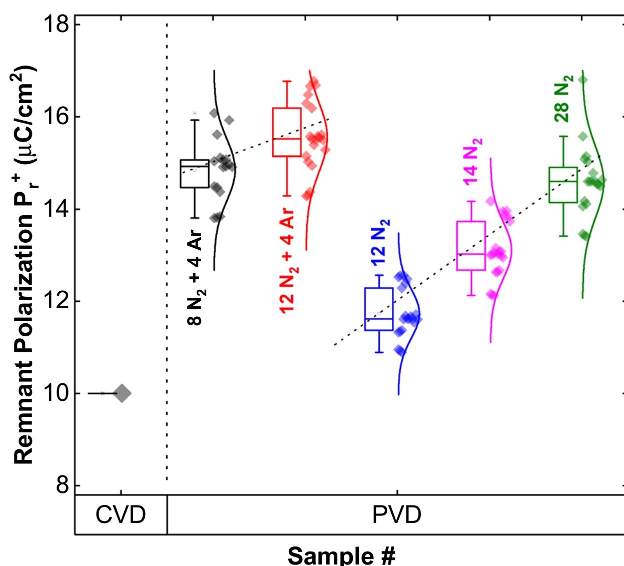

Fig. 4 Remanent polarization of MFM capacitors with different TiN TE deposited via CVD or PVD. In the case of PVD, the different process gas flows are given next to the respective box plot in sccm. Each box plot consists of 40 devices measured after 10^4 wake-up cycles at a maximum field of 3 MV/cm. In the case of the CVD TE, one device was measured after 10^4 wake-up cycles at a limited maximum field of 2.5 MV/cm

Acknowledgments This work received funding within the ECSEL Joint Undertaking project WAKeMeUP in collaboration with the European Union's H2020 Framework Program (Grant No. H2020/2014-2020) and National Authorities, under Grant Agreement Number 783176.

Funding Open Access funding enabled and organized by Projekt DEAL.

Data availability The datasets generated during and/or analyzed during the current study are available from the corresponding author on reasonable request.

Declarations

Conflict of interest The authors declare that they have no conflict of interest.

Open Access This article is licensed under a Creative Commons Attribution 4.0 International License, which permits use, sharing, adaptation, distribution and reproduction in any medium or format, as long as you give appropriate credit to the original author(s) and the source, provide a link to the Creative Commons licence, and indicate if changes were made. The images or other third party material in this article are included in the article's Creative Commons licence, unless indicated otherwise in a credit line to the material. If material is not included in the article's Creative Commons licence and your intended use is not permitted by statutory regulation or exceeds the permitted use, you will

need to obtain permission directly from the copyright holder. To view a copy of this licence, visit http://creativecommons.org/licenses/by/4.0/.

References

1. A. Keshavarzi, W. van den Hoek, IEEE Design Test. **36**(2), 41 (2019). https://doi.org/10.1109/MDAT.2019.2899075
2. A. Keshavarzi, K. Ni, W. van den Hoek, S. Datta, A. Raychowdhury, IEEE Micro **40**(6), 33 (2020). https://doi.org/10.1109/MM.2020.3026667
3. N. Setter, D. Damjanovic, L. Eng, G. Fox, S. Gevorgian, S. Hong, A. Kingon, H. Kohlstedt, N.Y. Park, G.B. Stephenson, I. Stolitchnov, A.K. Taganstev, D.V. Taylor, T. Yamada, S. Streiffer, J. Appl. Phys. **100**(5), 051606 (2006). https://doi.org/10.1063/1.2336999
4. J. Müller, T.S. Böscke, U. Schröder, S. Mueller, D. Bräuhaus, U. Böttger, L. Frey, T. Mikolajick, Nano Lett. **12**(8), 4318 (2012). https://doi.org/10.1021/nl302049k
5. S.J. Kim, J. Mohan, S.R. Summerfelt, J. Kim, JOM **71**(1), 246 (2019). https://doi.org/10.1007/s11837-018-3140-5
6. M. Lederer, T. Kämpfe, R. Olivo, D. Lehninger, C. Mart, S. Kirbach, T. Ali, P. Polakowski, L. Roy, K. Seidel, Appl. Phys. Lett. **115**(22), 222902 (2019). https://doi.org/10.1063/1.5129318
7. D. Lehninger, R. Olivo, T. Ali, M. Lederer, T. Kämpfe, C. Mart, K. Biedermann, K. Kühnel, L. Roy, M. Kalkani, K. Seidel, Physica Status Solidi (A) **217**(8), 1900840 (2020). https://doi.org/10.1002/pssa.201900840
8. D. Lehninger, T. Ali, R. Olivo, M. Lederer, T. Kampfe, K. Mertens, K. Seidel, in *2020 Joint Conference of the IEEE International Frequency Control Symposium and International Symposium on Applications of Ferroelectrics (IFCS-ISAF)* (IEEE, 2020), pp. 1–3. https://doi.org/10.1109/IFCS-ISAF41089.2020.9234879
9. D. Lehninger, M. Ellinger, T. Ali, S. Li, K. Mertens, M. Lederer, R. Olivio, T. Kämpfe, N. Hanisch, K. Biedermann, M. Rudolph, V. Brackmann, S. Sanctis, M.P.M. Jank, K. Seidel, Adv. Electron. Mater. **58**, 2100082 (2021). https://doi.org/10.1002/aelm.202100082
10. J. Hur, Y.C. Luo, N. Tasneem, A.I. Khan, S. Yu, IEEE Trans. Electron Devices **39**, 1–5 (2021)
11. M.H. Park, Y.H. Lee, H.J. Kim, T. Schenk, W. Lee, K.D. Kim, F.P.G. Fengler, T. Mikolajick, U. Schroeder, C.S. Hwang, Nanoscale **9**(28), 9973 (2017). https://doi.org/10.1039/C7NR02121F
12. P. Kelly, R. Arnell, Vacuum **56**(3), 159 (2000). https://doi.org/10.1016/S0042-207X(99)00189-X
13. M. Lederer, R. Olivo, D. Lehninger, S. Abdulazhanov, T. Kämpfe, S. Kirbach, C. Mart, K. Seidel, L.M. Eng, physica status solidi (RRL) - Rapid Research Letters (2021). https://doi.org/10.1002/pssr.202100086
14. M. Lederer, T. Kämpfe, N. Vogel, D. Utess, B. Volkmann, T. Ali, R. Olivo, J. Müller, S. Beyer, M. Trentzsch, K. Seidel, Eng, L. M., Nanomaterials (Basel, Switzerland) **10**(2) (2020). https://doi.org/10.3390/nano10020384
15. T. Schenk, E. Yurchuk, S. Mueller, U. Schroeder, S. Starschich, U. Böttger, T. Mikolajick, Appl. Phys. Rev. **1**(4), 041103 (2014). https://doi.org/10.1063/1.4902396